Continuous wave and tunable laser operation of Yb^{3+} in disordered $NaLa(MoO_4)_2$

M. Rico,[1] J. Liu,[1] J. M. Cano-Torres,[2] A. García-Cortés,[2] C. Cascales,[2] C. Zaldo,[2]

U. Griebner,[1] V. Petrov[1,✉]

[1]Max-Born-Institute for Nonlinear Optics and Ultrafast Spectroscopy,

2A Max-Born-Str., D-12489 Berlin, Germany

[2]Instituto de Ciencia de Materiales de Madrid, Consejo Superior de Investigaciones Científicas, c/ Sor Juana Inés de la Cruz 3, Cantoblanco, E-28049 Madrid, Spain

✉ Fax: +49-30/63921289, E-mail: petrov@mbi-berlin.de

ABSTRACT: Continuous-wave Yb^{3+} laser operation is studied in single crystals of disordered $NaLa(MoO_4)_2$ at room temperature. The sample used was grown by the Czochralski technique and incorporates an Yb ion density of 3.1×10^{20} cm^{-3}. The effect of the Yb concentration on some of the crystal properties is described as well as the spectroscopic Yb^{3+} properties at 5 K. Maximum slope efficiencies of about 40 % for π and 38 % for σ polarization were obtained under Ti:sapphire laser pumping near 976 nm, respectively. The maximum output power for the π polarization was 400 mW at 1039.5 nm, the threshold in this case amounted to 240 mW (absorbed pump power). The laser emission was tunable between 1016 and 1064 nm with a Lyot filter. Lasing was also realized by pumping with a fiber-coupled diode laser module. Maximum output power of 900 mW at 1035 nm was achieved in this case for the π polarization and the threshold was 280 mW. The results, in terms of output power and tunability, are superior in comparison to all previous reports on Yb-doped disordered double tungstate or molybdate crystals and represent a significant improvement in comparison to earlier experiments with low-doped $Yb:NaLa(MoO_4)_2$.

PACS 42.55.Rz; 42.55.Xi; 42.70.Hj

1. Introduction

Most of the widespread femtosecond laser systems nowadays available are based on the Ti^{3+} emission in sapphire in the 700-1100 nm spectral range which requires pumping in the green provided by Ar^{+} or frequency doubled Nd^{3+}-lasers. However, current laser technologies tend to direct pumping by semiconductor diode lasers. Suitable ions for this purpose are some of the lanthanides, e.g. Nd^{3+}, Tm^{3+} and Yb^{3+}. To support ultrashort laser pulses, media with broad optical emission bands are required. Usually this is associated with broader absorption lines which relaxes the requirements to the pump laser diodes. Such broad bands are found either when an electron-lattice vibrations coupling occurs or when a site distribution of the optically active ion exists. Yb^{3+} has attracted considerable attention in this respect for the 1 μm spectral range since: due to the strong electron–phonon coupling to the lattice, it exhibits linewidths which are intrinsically broader than the Nd^{3+} ion. Moreover, Yb^{3+} possesses longer energy-storage lifetime and smaller quantum defect than Nd^{3+}, and it can be pumped by the optically more robust InGaAs diode lasers operating in the 900–1000 nm spectral range. Finally, the relatively simple two-manifold structure of Yb^{3+} prohibits undesired excited state absorption, up-conversion and cross-relaxation processes. Notwithstanding all these attractive features, the bandwidth of Yb^{3+} still remains substantially narrower than that of Ti^{3+}:sapphire and in general it is difficult to produce sub-100 fs pulses with lasers based on ytterbium doped crystals.

Most recently, both Ti:sapphire and diode pumped laser operation was demonstrated for three Yb-doped sodium double tungstate and molybdate crystals with tetragonal crystalline structure, belonging to a series with the general formula $NaT(XO_4)_2$ where T is a trivalent ion and X=W or Mo [1-5]. The interest in these crystals is motivated by the fact that in the tetragonal phase, Na and T cations are randomly distributed over the same cationic sublattice leading to a local lattice disorder around the optically active ions, like Yb^{3+}. This

disorder along with the Yb^{3+} phonon coupling could potentially ensure the large bandwidths needed in tunable and mode-locked diode pumped solid-state lasers.

Most of the double tungstate and molybdate compounds undergo polymorphic transformations upon cooling to room temperature which hampers the crystal growth procedures. For the Na-based tungstates and molybdates the polymorphic transformations observed are weak and the tetragonal phase formed from melt solidification is stable at room temperature, maybe only with some minor crystalline modifications. This is a further attractive feature since it allows the use of the Czochralski method for crystal growth.

The title compound, sodium lanthanum molybdate $NaLa(MoO_4)_2$, or shortly NaLaMo, was studied as a room temperature laser host for the Nd^{3+} ion almost 40 years ago. Lamp-pumped operation of Nd:NaLaMo was demonstrated not only in the pulsed regime at 1059.5–1065.3 nm [6,7] and 1338–1344 nm [8], but also in the continuous-wave (cw) regime at 1065.3 nm [9]. In addition NaLaMo, which is an efficient Raman active medium [10], when doped with Nd^{3+}, was shown to be an efficient self-converting Raman crystal both in the picosecond [11] and in the nanosecond regime [12].

In 2005, initial results on the room temperature cw laser operation of Yb:NaLaMo were independently reported for Ti-sapphire pumping with a crystal of 1.3×10^{20} cm^{-3} Yb-ion concentration [2] and laser diode pumping of a sample doped with 0.9×10^{20} cm^{-3} ytterbium [3]. In the present work we demonstrate substantial improvement of the Yb:NaLaMo laser performance at room temperature and without active cooling, both under Ti:sapphire and diode laser pumping, using 2.5-3 times higher Yb^{3+} doping level. We provide also information on the crystal growth conditions and some relevant new optical and spectroscopic properties.

2. Crystal growth and spectroscopy of Yb-doped $NaLa(MoO_4)_2$

The Yb:NaLaMo crystals were grown in air by the Czochralski method using a pulling equipment and a Si_2Mo heating resistance, with Pt crucibles and seeding with a Pt wire. The pulling rate was 2 mm/h and the seed rotation rate - 8-20 rpm. Crystals with three Yb doping levels (3, 8 and 10 mol% in the melt) could be successfully grown with sufficient optical quality and size of several cm^3.

In the growth experiences, the melting/solidification temperature was observed to decrease with the Yb concentration. Simultaneous thermogravimetric (TG) and differential thermal analyses (DTA) were made in air using Al_2O_3 as a reference. The heating and cooling ramps were at a rate of 10ºC/min. In order to assess the melting character, the samples were subjected to two consecutive melting/resolidification cycles. The results are shown in Fig. 1. The main endothermic and exothermic peaks associated with melting and resolidification occur at the same temperature independently of the thermal history of the samples. This indicates the congruent melting character. For the 10 mol% Yb in the melt doped sample, this temperature was 1150±2ºC. However, significant weight loss takes place close or above the melting temperature. This is attributed to evaporation, as already observed in other molybdates [13].

The Yb concentrations [Yb] estimated by inductively coupled plasma (ICP) emission, independently for the three Yb doping levels (Table 1), yielded a segregation coefficient of $K=[Yb]_{crystal}/[Yb]_{melt}$ in the 0.35-0.5 range.

The lattice parameters were derived from Rietveld profile fits [14] of X-ray θ-2θ powder diffraction patterns collected at room temperature. For this purpose the samples were ground and mixed with W as a standard [15]. The lattice cell parameters of the tetragonal Yb:NaLaMo crystals are summarized in Table 1. A reduction of the cell volume obviously takes place upon increasing Yb concentration in the crystal, which can be described as:

a(Å)=5.3431-2.2×10^{-23}[Yb] and c(Å)=11.741-6×10^{-23}[Yb], where [Yb] is expressed in cm^{-3}. The crystal lattice parameters extrapolated for NaLaMo agree with those obtained for low (0.1%) Nd-doped NaLaMo [16].

The spectroscopic information available on Yb^{3+} in NaLaMo is limited to room temperature measurements. Peak absorption cross sections of 2.4-2.5×10^{-20} cm^2 for the π and 1.5-1.8×5x10^{-20} cm^2 for the σ polarization were reported at 977 nm [3,17]. From powder measurements, the fluorescence lifetime of the excited $^2F_{5/2}$ multiplet of Yb^{3+} in NaLaMo amounts to 280-284 μs [3,17].

Yb^{3+} operates as a quasi 3-level laser; therefore large splitting of the ground $^2F_{7/2}$ manifold is desirable. In order to evaluate this splitting and to describe the origin of the structure observed in optical absorption and photoluminescence measurements at 300 K we measured the spectroscopic properties at 5 K. Figure 2 shows the results for the 10 mol % (in the melt) Yb-doped NaLaMo together with the Stark level positions. The band observed at 10256 cm^{-1} both in absorption and emission spectra is ascribed to the $^2F_{7/2}(0) \leftrightarrow {}^2F_{5/2}(0')$ transition (zero-phonon line). The FWHM of this main absorption band (≈11 cm^{-1}) substantially exceeds the bandwidth observed for the equivalent Yb^{3+} transition in ordered double tungstate crystal hosts with unique site for Yb^{3+}, e.g. $KGd(WO_4)_2$, for which the FWHM amounts to 3.5 cm^{-1}. Therefore, the contribution from different Yb^{3+} environments in the disordered NaLaMo host is essential for the observed bandwidth. Bands which appear either overlapped or well resolved with energy separations >11 cm^{-1} should have a different origin. This is most likely due to electron-phonon coupling of the crystal field levels with the vibrating environment. Assuming a phonon energy of about 40 cm^{-1}, bands associated with non-crystal field levels can be tentatively identified as summarized by the arrows in Fig. 2.

3. Laser experiments

All laser experiments hereafter described were conducted at room temperature with an uncoated 2.59 mm thick, *a*-cut plate sliced from the 10 mol% (in the melt) Yb-doped NaLaMo crystal. The sample was mounted on a copper holder without active cooling. Two different pump sources were applied: a widely tunable cw Ti:sapphire laser and a fiber-coupled diode laser module. The latter had a 116 μm fiber core diameter with a numerical aperture of 0.2 and provided a maximum unpolarized and multiline output of 7 W in the wavelength range 974 – 980 nm.

A three-mirror astigmatically compensated laser cavity (Fig. 3a) was used for Ti:sapphire laser pumping. It consisted of an end mirror M_1 with radius of curvature RC=-5 cm, a folding mirror M_2 with RC=-10 cm, through which the pump beam was focused by a f=6.28 cm lens L, and a plane output coupler (M_3) of transmission T_{OC}. The total cavity length was 74 cm. The pump beam focal spot had a Gaussian waist of about 22 μm and the pump power incident onto the crystal was limited to 2.6 W.

The optimum pump wavelengths for the π (E//c) and σ (H//c) orientations of the Yb:NaLaMo crystal under Brewster angle, were 976.7 and 975.8 nm, respectively, which corresponds to the maxima in the absorption spectra. Figure 4 shows the change of the actual absorption with the incident pump power P_{INC}. At maximum P_{INC}, the Yb^{3+} absorption was bleached down to ≈ 45% for the π and down to 35% for the σ polarization. However, laser operation had a recycling effect resulting in recovery of the absorption depending on the intracavity intensity and hence on the output coupler used. In the case of π-polarization the absorption increased almost to its initial small signal value (the one measured by a spectrophotometer and corrected for the Brewster geometry).

Figure 5 shows the laser performance obtained. For the π polarization (Fig. 5a), a maximum output power of 400 mW was achieved at 1039.5 nm by using T_{OC}=1.1%. In this

case, the laser threshold and the slope efficiency were 240 mW (absorbed pump power) and 27.5%, respectively. The decrease of the output laser power for T_{OC}=2.8, 5.5 and 10%, can be partially attributed to the reduced recycling effect and crystal absorption. In particular, for T_{OC}=10% this can be clearly observed in Fig. 4. The slope efficiency is not affected by this effect since it is calculated with respect to the absorbed power: it was maximum (39.7%) for T_{OC}=5.5%. The pump and slope efficiencies were lower for the σ polarization (Fig. 5b), which can be attributed to the lower cross sections, and the laser wavelengths were also slightly shifted.

Wavelength tunability was studied by inserting a two-plate Lyot filter under Brewster angle in the M_2-M_3 cavity arm (Fig. 3a). Under optimum alignment the power reduction with the filter inside the cavity did no exceed 5%. Figure 6 shows the tunability of the Yb:NaLaMo laser output for an incident pump power of 2.3 W and two different output couplers, T_{OC}=1.1% and 5.5%. The tuning curves depend both on the laser gain and loss mechanisms and in the best case extend from 1016 to 1064 nm. The FWHM of 33 nm corresponds to $\Delta\nu$=9.1×10^{12} Hz which means, for a sech^2 or Gaussian pulse shape, that potentially sub-50 fs pulses could be supported in the mode-locking regime.

The diode pumping experiments were performed with the nearly hemispherical cavity schematically shown in Fig. 3b. M_1 was a plane high reflector for the laser wavelength (1020-1200 nm) on a 3-mm thick quartz substrate which was highly transmitting near 980 nm. For the other cavity mirror (OC) concave output couplers with RC=-5 cm and four selectable transmission levels, T_{OC}=0.5%, 1%, 2%, and 3%, were available. The sample was placed as close as possible (≈0.2 mm) to M_1. In order to match the calculated fundamental cavity mode size the unpolarized diode laser output was focused by a f = 6.2 mm microoptics to a spot size of ≈40 μm (Gaussian waist) in the position of the Yb:NaLaMo crystal.

A maximum output power of 0.9 W at 1035 nm was obtained with the diode pumped laser configuration for T_{OC}= 1%. T_{OC}=0.5, 1% and 2% led to similar output power levels (0.84, 0.90 and 0.81 W, respectively) and shifts in the laser wavelength (see Fig. 7) as in the case of Ti:sapphire laser pumping. The minimum absorbed pump power at the laser threshold was 280 mW for T_{OC}=0.5 %. In all cases the polarization of the output beam was parallel to the crystal *c*-axis (π) due to the higher gain.

Using higher output coupling (T_{OC}=3%) resulted in lower output powers (Fig. 7) which could be partially due to the reduced recycling effect and crystal absorption. However, in this cavity configuration, the large divergence of the pump source did not allow to measure the absorbed pump power under lasing conditions. While this could be done for the estimation of the saturation effect (Fig. 7) and the threshold only with the output coupler removed, in the general case the efficiencies had to be calculated with respect to the incident pump power (Fig. 7) and were correspondingly lower. It should be also noted that the pump spectral distribution changes slightly with the power (diode laser current).

Table 2 shows a comparison of the laser performance achieved so far in the Yb-doped disordered double tungstates and molybdates [1-5]. This work presents the best results up to now in terms of maximum output power and tunability under Ti-sapphire pumping. The former holds also for the case of diode pumping where a 4-fold increase in the output power is achieved in comparison to previous work on Yb:NaLaMo [3]. The improved results can be partially associated with the higher ytterbium concentration now used and the superior optical quality. The latter is a crucial point since defects appearing for increasing Yb concentrations deteriorate the crystal optical quality.

4. Conclusion

In conclusion, disordered crystals of $NaLa(MoO_4)_2$ with tetragonal structure were successfully grown by the Czochralski method with up to 5.1 mol% Yb-doping in the crystal and good enough optical quality. This is attributed to the congruent melting character preserved for this dopant level. The crystal field splitting of the Yb^{3+} multiplets is only slightly lower than that observed in monoclinic double tungstates. This splitting is sufficient to allow efficient room temperature and tunable cw laser operation under Ti:sapphire or diode laser pumping. The slope efficiency reached ≈40 % and output powers as high as 900 mW could be achieved for the π polarization without special cooling. The 48 nm wide tunability range is promising for passively mode-locked operation in the sub-50 fs regime.

Acknowledgements

This work was supported by the projects DT-CRYS, NMP3-CT-2003-505580 (EU), MAT 2002-4605-C05-05 and CAM-MAT-434-2004 (Spain). Dr. M. Rico thanks the Education and Culture Ministry of Spain for financial support. The cooperation of Dr. V. Volkov in the early stage of this work is also acknowledged.

References:

[1] M. Rico, J. Liu, U. Griebner, V. Petrov, M. D. Serrano, F. Esteban-Betegon, C. Cascales, C. Zaldo: Opt. Exp. **12**, 5362 (2004).

[2] J. Liu, J. M. Cano-Torres, C. Cascales, F. Esteban-Betegón, M. D. Serrano, V. Volkov, C. Zaldo, M. Rico, U. Griebner, V. Petrov: phys. stat. sol. (a) **202**, R29 (2005).

[3] A. S. Yasukevich, A. V. Mandrik, V. E. Kisel, V. G. Shcherbitsky, G. N. Klavsut, N. V. Kuleshov, A. A. Pavlyuk: Advanced Solid-State Photonics 2005, Feb.6-9, Vienna, Austria, Technical Digest (CD ROM), Paper MB6.

[4] J. Johannsen, M. Mond, K. Petermann, G. Huber, L. Ackermann, D. Rytz, C. Dupre, Advanced Solid-State Photonics 2005, Feb.6-9, Vienna, Austria, Technical Digest (CD ROM), Paper MB44.

[5] J. Liu, J. M. Cano-Torres, F. Esteban-Betegón, M. D. Serrano, C. Cascales and C. Zaldo, M. Rico, U. Griebner, V. Petrov: Opt. Las. Techn. (2005) submitted.

[6] A. M. Morozov, M. N. Tolstoi, P. P. Feofilov, V. N. Shapovalov: Opt. Spectrosc. **22**, 224 (1967) [transl. from Opt. Spektrosk. **22**, 414 (1967).

[7] G. M. Zverev, G. Ya. Kolodny: Sov. Phys. JETP **25**, 217 (1967) [transl. from Zh. Eksp. Teor. Fiz. **52**, 337 (1967)].

[8] A. A. Kaminskii, S. E. Sarkisov: Sov. J. Quantum Electron. **3**, 248 (1973) [transl. from Kvantovaya Elektron. (Moscow) No. 3(15), 106 (1973).

[9] A. A. Kaminskii, G. Ya. Kolodyni, N. I. Sergeeva: J. Appl. Spectr. (USSR) **9**, 1275 (1968). [transl. from Zh. Prikl. Spektrosk. **9**, 884 (1968)].

[10] A. A. Kaminskii, S. N. Bagaev, D. Grebe, H. J. Eichler, A. A. Pavlyuk, R. Macdonald: Quantum Electron. **26**, 193 (1996) [transl. from Kvantovaya Elektronika (Moscow) **23**, 199 (1996)].

[11] J. Viscakas, V. Syrusas: Sov. Phys. – Collection **27**, 31 (1987) [transl. from Litovskii Fiz. Sbornik **27**, 547 (1987)].

[12] A. V. Gulin, V. A. Pashkov, N. S. Ustimenko: Proc. SPIE **4350**, 36 (2001).

[13] V. Volkov, M. Rico, A. Méndez-Blas, C. Zaldo: J. Phys. Chem. Sol. **63**, 95 (2002).

[14] T. Roisnel, J. Rodríguez-Carvajal, WinPLOTR. http://www-llb.cea.fr/fullweb/winplotr/winplotr.htm.

[15] W. Parrish: Acta Cryst. **13**, 838 (1960).

[16] S. B. Stevens, C. A. Morrison, T. H. Allik, A. L. Rheingold, B. S. Haggerty. Phys. Rev. B **43**, 7386 (1991).

[17] Yu. K. Voron'ko, E. V. Zharikov, D. A. Lis, A. A. Sobol, K. A. Subbotin, S. N. Ushakov, V. E. Shukshin: Proc. SPIE **5478**, 60 (2004).

Table 1: Lattice cell parameters of Yb-doped $NaLa(MoO_4)_2$ crystals.

mol % Yb		$[Yb]_{crystal}$	*a*	*c*	*V*
melt	crystal	($10^{20}cm^{-3}$)	(Å)	(Å)	(Å^3)
3	1.1	0.61	5.3420(4)	11.737(1)	334.93(5)
8	3.1	1.84	5.3387(4)	11.729(2)	334.28(6)
10	5.1	3.08	5.3365(5)	11.722(2)	333.82(6)

Table 2: Laser parameters achieved recently for disordered Yb-doped $NaGd(WO_4)_2$ (NaGdW), $NaLa(WO_4)_2$ (NaLaW), and $NaLa(MoO_4)_2$ (NaLaMo) crystals with the π polarization. [Yb]: Ytterbium concentration in the crystal, λ_P: pump wavelength, T_{OC}: output coupler transmission for maximum output power P_{max}, λ_L: lasing wavelength, $\Delta\lambda$: tunability range with Lyot filter.

Ti:sapphire laser pumping						**Diode laser pumping**			
Material	NaGdW	NaGdW	NaLaW	NaLaMo	NaLaMo	NaGdW	NaLaW	NaLaMo*	NaLaMo
[Yb] (10^{20} cm^{-3})	3.19	5.1	1.1	1.3	3.08	3.19	1.1	0.9	3.08
λ_P (nm)	975	973.6	976.6	976.6	976.7	≈ 975	≈ 976	980	≈ 976
T_{OC} (%)	0.81	10.0	1.1	3.0	1.1	0.71	1.0	1.0	1.0
P_{max} (mW)	230	336	205	120	400	227	330	220	900
λ_L (nm)	1023	1026.8	1034	1025	1039.5	1033	1031	1023	1035
$\Delta\lambda$ (nm)	-	33	40	38	48				
Ref.	[4]	[1]	[2]	[2]	This work	[4]	[5]	[3]	This work

* Crystal with active cooling.

Figure Captions

Figure 1. Thermogravimetric TG (dashed line) and differential thermal analysis DTA (solid line) of a 10 mol % (in the melt) Yb-doped $NaLa(MoO_4)_2$ crystal heated in air at 10ºC/min.

Figure 2. Absorption and emission spectra of $Yb:NaLa(MoO_4)_2$ recorded at 5 K. The absorption was measured both for the π (dashed line) and the σ (solid line) polarization while the unpolarized emission measurement is presented for excitation wavelengths of 960 nm (dashed line) and 974.2 nm (solid line). The determined crystal field $^2F_{5/2}$ and $^2F_{7/2}$ Stark energy levels are also given. The arrows indicate possible bands associated with coupling to $\hbar\omega$=40 cm^{-1} phonons.

Figure 3. Schematic of the laser setups: (a) Ti:sapphire laser pumped cavity. (b) Fiber-coupled diode laser pumped cavity.

Figure 4. Single pass absorption under laser operation (full symbols) and without lasing (open symbols) versus incident pump power P_{INC} using the Ti-sapphire laser pump source.

Figure 5. Output power versus absorbed pump power (symbols) for the Ti-sapphire pumped cw $Yb:NaLa(MoO_4)_2$ laser. The linear fits shown give the slope efficiencies, η, for the indicated output coupler transmittances T_{OC}.

Figure 6. Wavelength tunability of the $Yb:NaLa(MoO_4)_2$ laser under Ti:sapphire laser pumping for an incident pump power P_{INC}=2.3 W and different output couplers.

Figure 7. Output power of the cw $Yb:NaLa(MoO_4)_2$ laser obtained by diode laser pumping at λ_P=976 nm and crystal absorption (open circles) at this wavelength without lasing, versus incident pump power P_{INC}. The straight lines are the fits used to calculate the slope efficiencies η corresponding to the four output couplers (T_{OC}) used.

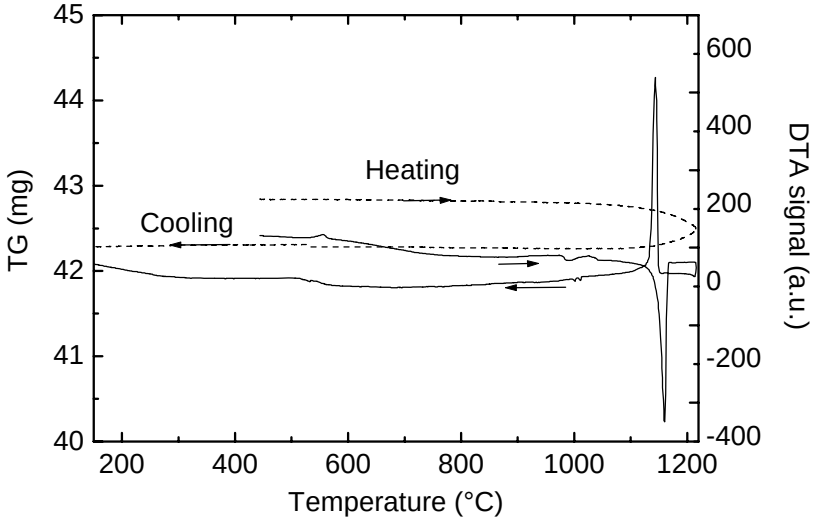
45
44
43
42
41
40
TG (mg)
600
400
200
0
-200
-400
DTA signal (a.u.)
Heating
Cooling
200
400
600
800
1000
1200
Temperature (°C)

Figure 1.

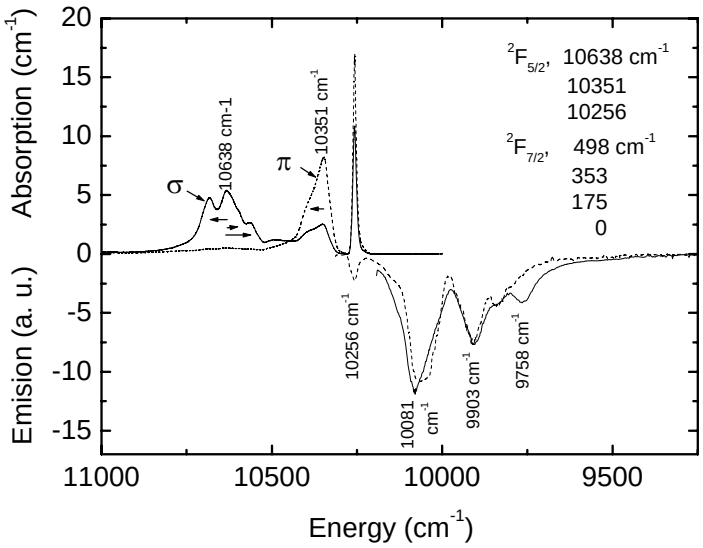
Absorption (cm-1)
Emision (a. u.)
Energy (cm-1)
σ
π
10638 cm-1
10351 cm-1
10256 cm-1
10081 cm-1
9903 cm-1
9758 cm-1
2F5/2, 10638 cm-1
10351
10256
2F7/2, 498 cm-1
353
175
0

Figure 2.

(a)

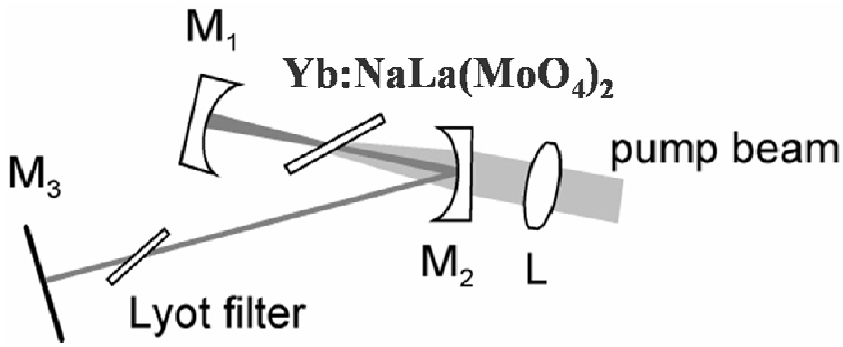
M1
Yb:NaLa(MoO4)2
pump beam
M3
M2
L
Lyot filter

(b)

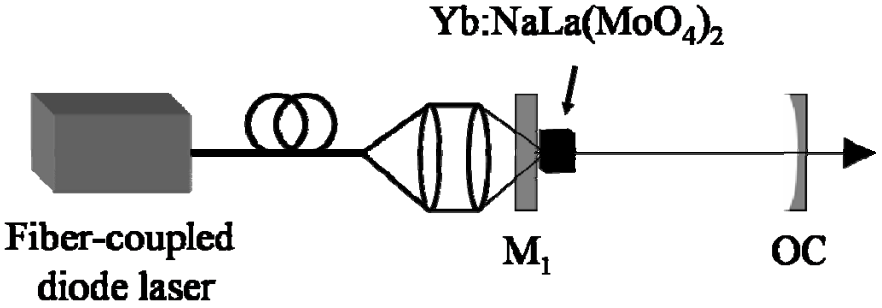
Yb:NaLa(MoO4)2
Fiber-coupled
diode laser
M1
OC

Figure 3.

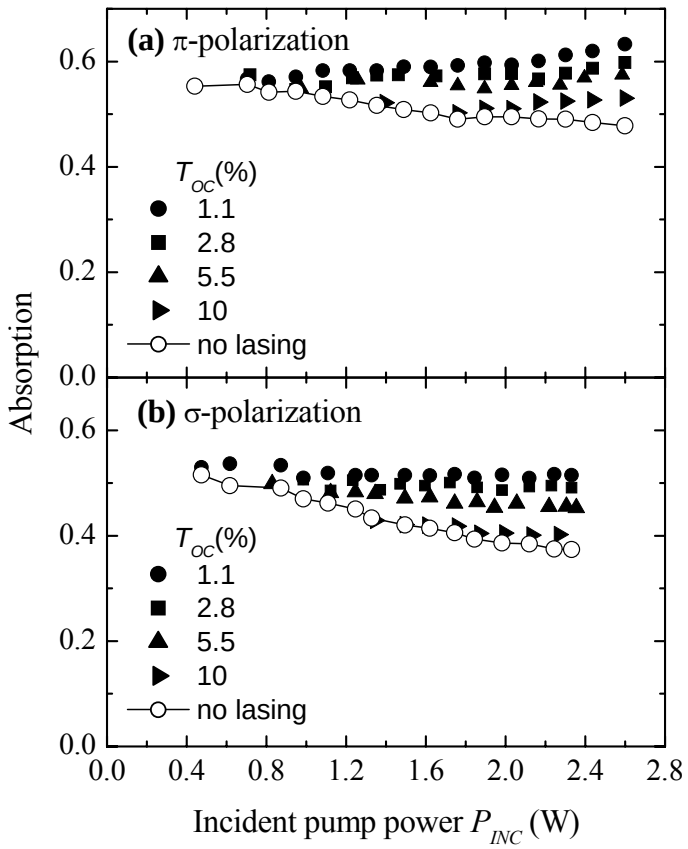
(a) π-polarization
T_{OC}(%)
1.1
2.8
5.5
10
no lasing
(b) σ-polarization
T_{OC}(%)
1.1
2.8
5.5
10
no lasing
Absorption
0.0
0.2
0.4
0.6
0.0
0.4
0.8
1.2
1.6
2.0
2.4
2.8
Incident pump power P_{INC} (W)

Figure 4.

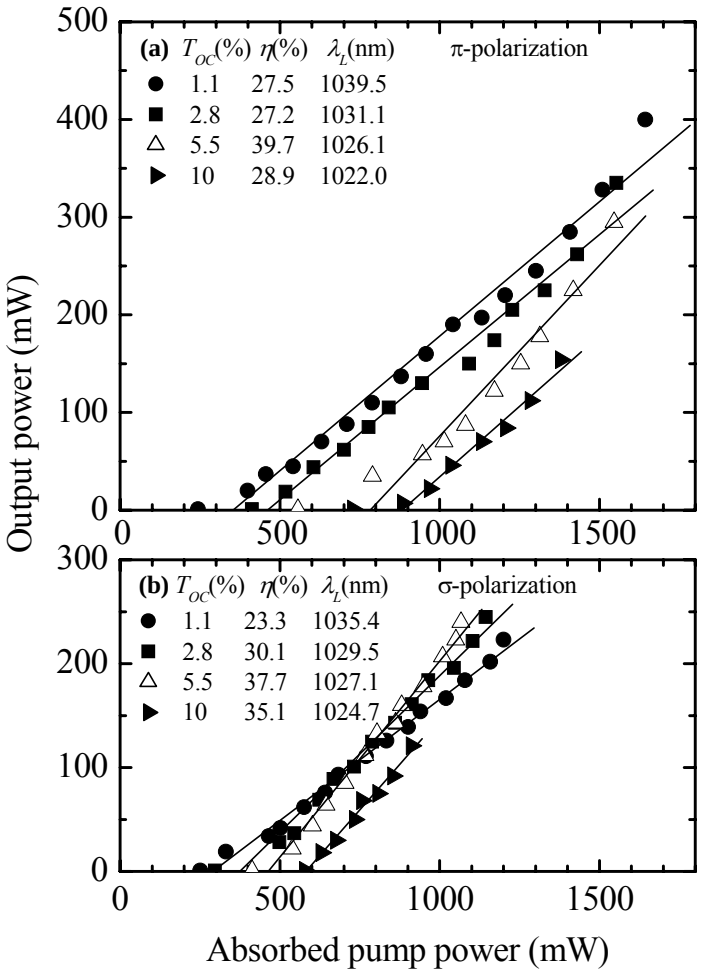
(a) T_{OC}(%) η(%) λ_L(nm) π-polarization
1.1 27.5 1039.5
2.8 27.2 1031.1
5.5 39.7 1026.1
10 28.9 1022.0
(b) T_{OC}(%) η(%) λ_L(nm) σ-polarization
1.1 23.3 1035.4
2.8 30.1 1029.5
5.5 37.7 1027.1
10 35.1 1024.7
Output power (mW)
Absorbed pump power (mW)
0
100
200
300
400
500
1000
1500

Fig. 5.

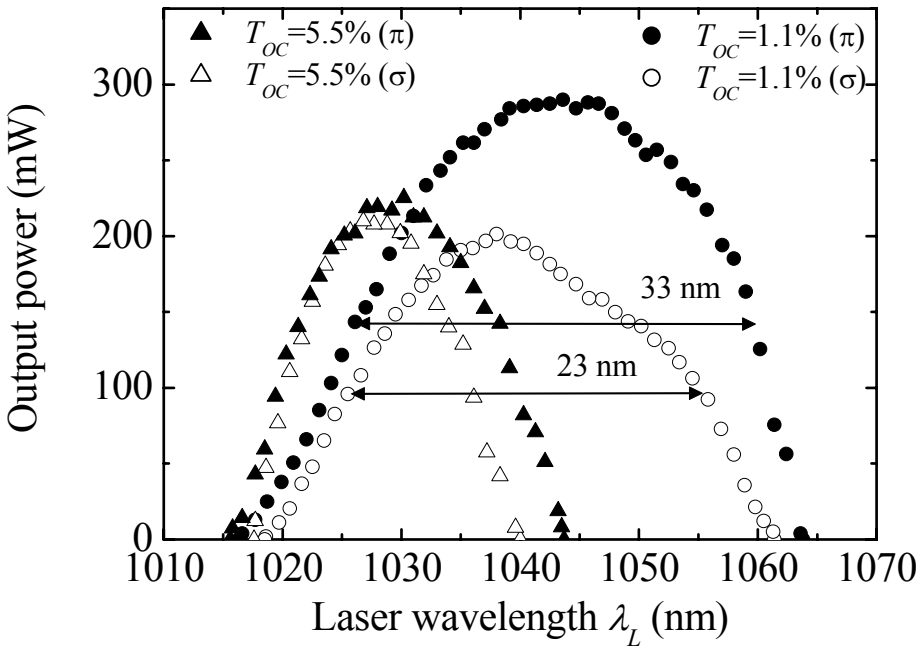
T_{OC}=5.5% (π)
T_{OC}=5.5% (σ)
T_{OC}=1.1% (π)
T_{OC}=1.1% (σ)
33 nm
23 nm
Output power (mW)
Laser wavelength λ_L (nm)
0
100
200
300
1010
1020
1030
1040
1050
1060
1070

Fig. 6.

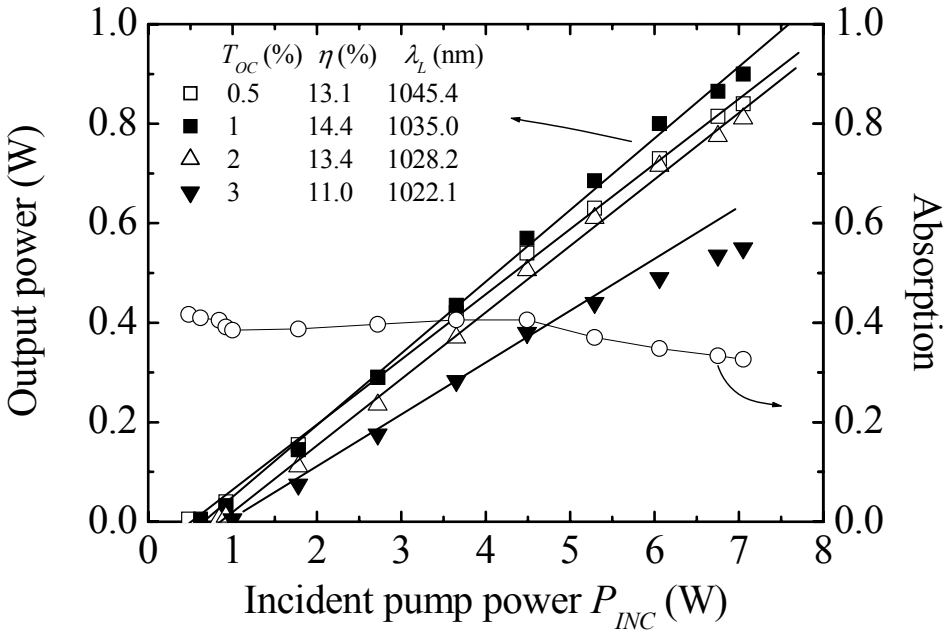
T_{OC} (%) η (%) λ_L (nm)
0.5 13.1 1045.4
1 14.4 1035.0
2 13.4 1028.2
3 11.0 1022.1
Output power (W)
Absorption
Incident pump power P_{INC} (W)
0.0
0.2
0.4
0.6
0.8
1.0
0
1
2
3
4
5
6
7
8

Fig. 7.